

The life cycle of a coherent Lagrangian Agulhas ring

Y. Wang¹, F. J. Beron-Vera² and M. J. Olascoaga¹

Abstract. We document the long-term evolution of an Agulhas ring detected from satellite altimetry using a technique from nonlinear dynamical systems that enables objective (i.e., observer-independent) eddy framing. Such objectively detected eddies have Lagrangian (material) boundaries that remain coherent (unfilamented) over the detection period. The ring preserves a quite compact material entity for a period of about 2 years even after most initial coherence is lost within 5 months after detection. We attribute this to the successive development of short-term coherent material boundaries around the ring. These boundaries provide effective short-term shielding for the ring, which prevents a large fraction of the ring's interior from being mixed with the ambient turbulent flow. We show that such coherence regain events cannot be inferred from Eulerian analysis. This process is terminated by a ring-splitting event which marks the ring demise, near the South American coast. The genesis of the ring is characterized by a ring-merging event away from the Agulhas retroflection, followed by a 4-month-long partial coherence stage, scenario that is quite different than a simple current occlusion and subsequent eddy pinch off.

1. Introduction

The long-term ability of Agulhas rings detected from satellite altimetry measurements of sea surface height (SSH) to maintain Lagrangian (i.e., material) coherence has been demonstrated using satellite ocean color imagery [Lehahn *et al.*, 2011]. This suggests a long-term transport ability for such rings, which has been the subject of recent investigation using nonlinear dynamical systems techniques that enable objective (i.e., observer-independent) framing of Lagrangian coherence. Using the over two-decade-long altimetry record, Wang *et al.* [2015] found that long-lived (of up to at least 1 year of duration) rings have small (about 50 km in diameter) coherent Lagrangian cores, suggesting a fast decay for the rings. On the other hand, they found that such cores carry a small (about 30%) fraction of water traceable into the Indian Ocean. The two findings together question the long-range ability of rings in transporting Agulhas leakage. In turn, Froyland *et al.* [2015] found that the rings decay slowly, enabling long-range Agulhas leakage transport, and that this is inferable from the Eulerian footprints of the rings on SSH.

The goal of the present paper is to bridge the gap between the above seemingly contradicting results by carrying out a detailed objective investigation of the genesis, evolution, and decay of the ring priorly investigated by Froyland *et al.* [2015]. This is done using Haller and Beron-Vera's [2013; 2014] technique, which enables optimal detection of rings with Lagrangian boundaries that exhibit no signs of filamentation over the coherence assessment time interval.

Lagrangian coherence is found to emerge quite spontaneously from turbulence, process that differs from the idealized scenario in which an Agulhas ring forms as a result of the occlusion of, and subsequent pinch off from, the Agulhas retroflection. This initial coherence is rapidly lost within

the Cape Basin, which is in line with the fast decay of the ring's SSH anomaly amplitude. Beyond the Walvis Ridge a large fraction of the ring (about 6×10^4 km³, corresponding to a 2-km-deep, 200-km-diameter ring) is observed to preserve a compact Lagrangian entity far beyond the theoretical Lagrangian coherence horizon. This is shown to be caused by successive short-term coherence regain events. Demise of the ring eventually occurs, triggered by a ring splitting event, after a rapid decay of the area enclosed by the short-term coherent Lagrangian loops that provided the interior fluid shielding from turbulent mixing with the ambient fluid along the ring path. Not all of these aspects of the evolution of the ring are inferable from Eulerian analysis of SSH, which although signals coherence gain upon crossing the Walvis Ridge, suggests slow decay thereafter. It is noted finally that even if this behavior generalizes to all Agulhas rings, which needs to be verified, their long-range transport ability is still limited.

The rest of the paper is organized as follows. Geodesic eddy detection is briefly reviewed in Section 2, which contains basic information of the altimetry dataset and some numerical details. The life cycle of the ring is described in Sections 3–5. Implications for transport are discussed in Section 6. Finally, Section 7 includes concluding remarks.

2. Geodesic eddy detection

We are concerned with fluid regions enclosed by exceptional material loops that defy the exponential stretching that a typical loop will experience in turbulent flow. As Haller and Beron-Vera [2013, 2014] have shown, such loops have small annular neighborhoods exhibiting no leading-order variation in averaged material stretching.

¹Department of Ocean Sciences, Rosenstiel School of Marine and Atmospheric Science, University of Miami, Miami, Florida, USA.

²Department of Atmospheric Sciences, Rosenstiel School of Marine and Atmospheric Science, University of Miami, Miami, Florida, USA.

More specifically, solving this variational problem reveals that the loops in question are uniformly stretching: any of their subsets are stretched by the same factor λ under advection by the flow from time t_0 to time t . The time t_0 positions of λ -stretching material loops turn out to be limit cycles of one of the following two equations for parametric curves $s \mapsto x_0(s)$:

$$\frac{dx_0}{ds} = \sqrt{\frac{\lambda_2(x_0) - \lambda^2}{\lambda_2(x_0) - \lambda_1(x_0)}} \xi_1(x_0) \pm \sqrt{\frac{\lambda^2 - \lambda_1(x_0)}{\lambda_2(x_0) - \lambda_1(x_0)}} \xi_2(x_0). \quad (1)$$

Here $\lambda_1(x_0) < \lambda^2 < \lambda_2(x_0)$, where $\{\lambda_i(x_0)\}$ and $\{\xi_i(x_0)\}$, satisfying

$$0 < \lambda_1(x_0) \equiv \frac{1}{\lambda_2(x_0)} < 1, \quad \xi_i(x_0) \cdot \xi_j(x_0) = \delta_{ij} \quad i, j = 1, 2, \quad (2)$$

are eigenvalues and (normalized) eigenvectors, respectively, of the Cauchy–Green tensor,

$$C_{t_0}^t(x_0) := DF_{t_0}^t(x_0)^\top DF_{t_0}^t(x_0), \quad (3)$$

an objective (i.e., independent of the observer) measure of material deformation, where $F_{t_0}^t : x_0 \mapsto x(t; x_0, t_0)$ is the flow map that takes time t_0 positions to time t positions of fluid particles, which obey

$$\frac{dx}{dt} = v(x, t), \quad (4)$$

where $v(x, t)$ is a divergenceless two-dimensional velocity field.

Limit cycles of (1) either grow or shrink under changes in λ , forming smooth annular regions of nonintersecting loops. The outermost member of such a band of material loops is observed physically as the boundary of a *coherent Lagrangian eddy*. Limit cycles of (1) tend to exist only for $\lambda \approx 1$. Material loops characterized by $\lambda = 1$ resist the universally observed material stretching in turbulence: they reassume their initial arclength at time t . This conservation of arclength, along with enclosed area preservation (which holds by assumption), produces extraordinary coherence [Beron-Vera et al., 2013]. Finally, limit cycles of (1) are (null) geodesics of the generalized Green–Lagrange tensor $C_{t_0}^t(x_0) - \lambda^2 \text{Id}$, which must necessarily contain degenerate points of $C_{t_0}^t(x_0)$ where its eigenvector field is isotropic. For this reason the above procedure is known as *geodesic eddy detection*.

The specific form of the velocity field considered here is given by

$$v(x, t) = \frac{g}{f} \nabla^\perp \eta(x, t), \quad (5)$$

where g is the acceleration of gravity, f stands for Coriolis parameter, and $\eta(x, t)$ is the SSH, taken as the sum of a (steady) mean dynamic topography and the (transient) altimetric SSH anomaly. The mean dynamic topography is constructed from satellite altimetry data, in-situ measurements, and a geoid model [Rio and Hernandez, 2004]. The SSH anomaly is provided weekly on a 0.25° -resolution longitude–latitude grid. This is referenced to a 20-year (1993–2012) mean, obtained from the combined processing of data collected by altimeters on the constellation of available satellites [Le Traon et al., 1998].

For the purpose of the present investigation we have chosen to focus on the ring detected and tracked by Froyland et al. [2015] over the period 1999–2001. This ring was considered by Wang et al. [2015] in their coherent transport calculations. The numerical implementation of geodesic eddy detection is documented at length [Haller and Beron-Vera,

2013, 2014; Beron-Vera et al., 2015; Wang et al., 2015; Karasch et al., 2014] and a software tool is now available [Onu et al., 2015]. Here we set the grid width of the computational domain to 0.1 km containing the ring, which enabled us to push the Lagrangian coherence detectability horizon close to 1.5 years. All integrations were carried out using a step-adapting fourth/fifth-order Runge–Kutta method with interpolations done with a cubic method.

3. Lagrangian coherence detection

We begin by applying geodesic eddy detection on $t_0 = 31$ March 1999, date by which the ring in question is in a sufficiently mature Lagrangian coherence stage. On that date the ring is found inside the region indicated by the square in the left panel of Fig. 1a. Geodesic eddy detection was carried out over t_0 through $t = t_0 + T$ for Lagrangian coherence time scale T increasing from 30 d in steps of 30 d out to 480 d, the longest T from which it was possible to extract a coherent Lagrangian eddy boundary. This is a very long Lagrangian coherence time scale, consistent with the statement above that the ring is in a mature Lagrangian coherence stage on the detection date. In fact, building material coherence takes a few months, as we show in Section 5. Application of geodesic eddy detection as just described resulted in a nested family of Lagrangian boundaries with coherence time scale increasing inward.

The extracted boundaries are indicated in red on the detection date in Fig. 1a (the right panel shows a blow-up of the region indicated by the rectangle in the left panel). For each T considered there is a nested family of λ -loops; the loop shown is the outermost one in each family. For T between 30 and 210 d the loops have $\lambda = 1$; for T increasing from 210 d, λ increases from 1.05 to 1.75. Thus as T increases the largest fluid area enclosed by a coherent material loop shrinks and the ability of a loop to reassume its initial arclength diminishes, reflecting that the ring turns unstable after a sufficiently long time.

The outer, shorter-lived boundaries provide a shield to the inner, longer-lived boundaries surrounding the core of the coherent Lagrangian ring. This is evident in the successive advected images of the boundaries under the flow. These are shown in Figs. 1b–f on selected dates over more than 2 years of evolution (an animation including monthly snapshots is supplied as supporting information Movie 1 at <https://www.dropbox.com/s/s6qr2bkrqtiltkr/SII.mov?dl=0>). An advected boundary is depicted red when it is within its theoretical Lagrangian coherence horizon and light blue when is beyond it. As expected, no noticeable signs of filamentation are observed up to that time scale. The filamentation observed beyond the coherence horizon reveals that the evolution of the ring is characterized by a decay process

Fig. 1g shows the area enclosed by the largest coherent Lagrangian boundary as a function of the geographical longitude taken by the ring as it translates westward. Note the drop, nearly exponential, before the ring reaches the Walvis Ridge and the slow decay thereafter. Indeed, within the first 5 months the area changes from about 4.5×10^4 to 7.5×10^3 km² (or the mean diameter from roughly 240 to 100 km), yet over the following 11 months the area decays very slowly at a rate of no more than 15 km²d⁻¹ until vanishing. Nearly 90% of the ring interior loses its initial material coherence prior to crossing the Walvis Ridge.

The rapid decay of the ring’s material coherence is not reflected in the topology of the total altimetric SSH field, but is accompanied by a similar rapid decay in the SSH anomaly amplitude. This is illustrated in Fig. 2, which depicts instantaneous total SSH field streamlines (a) and maximum SSH anomaly (b) in the domains occupied by the ring indicated in Figs. 1a–f. First note that the streamlines are closed both before and after the ring crosses the Walvis Ridge, signaling

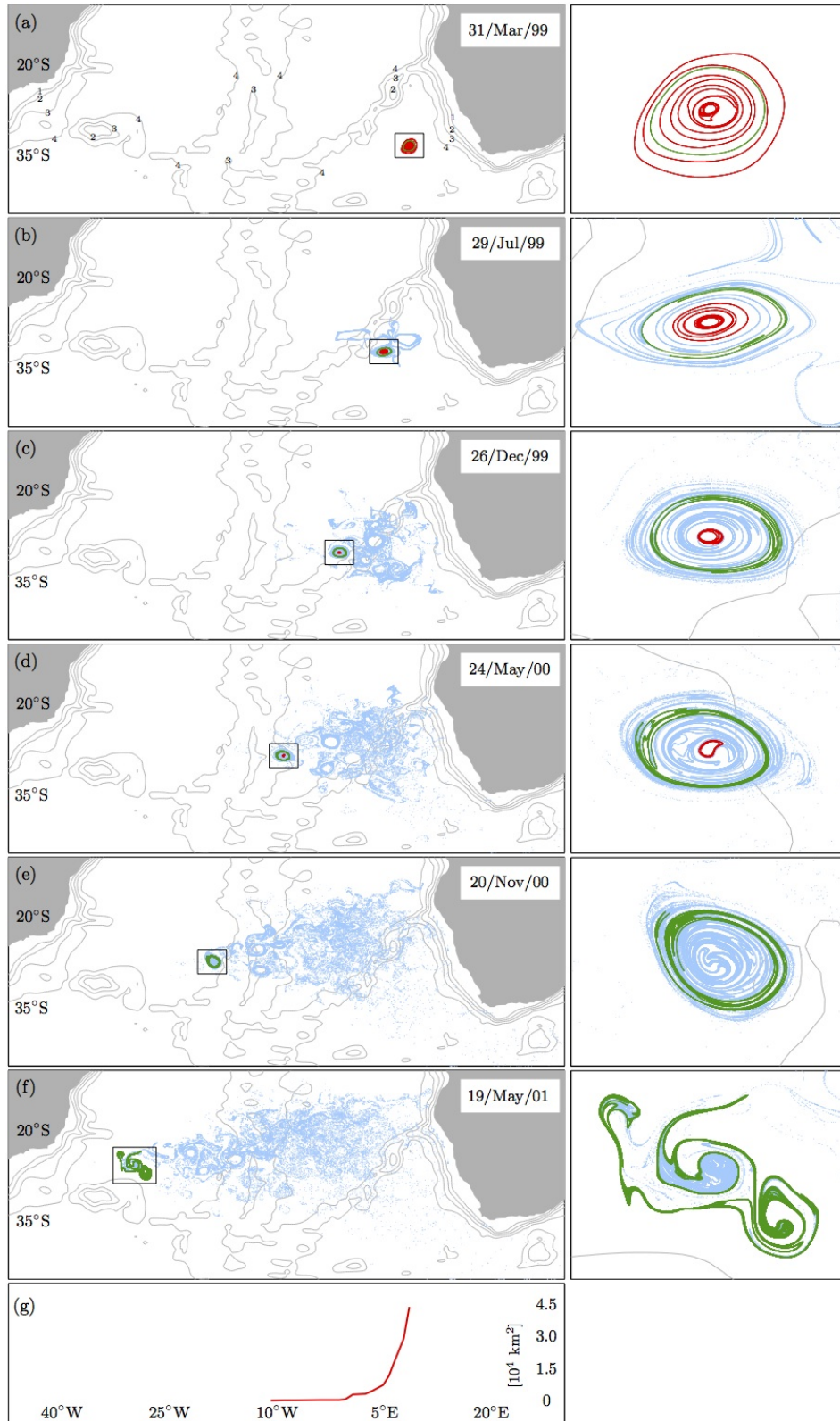


Figure 1. (a) Nested family of coherent Lagrangian ring boundaries extracted from altimetry-derived velocity by applying geodesic eddy detection on $t_0 = 31$ March 1999 inside the region indicated by a rectangle. Each member of the family has a different Lagrangian coherence time scale T ranging from 30 d (outermost) to 480 d (innermost) in steps of 30 d. Selected isobaths (in km) are indicated in gray. The outset is a blowup of the indicated region. (b–f) Advected images under the flow (i.e., evolution) of the coherent Lagrangian eddy boundaries in (a) on selected dates. An advected boundary is depicted red when it is within its theoretical Lagrangian coherence horizon and in a blue tone when is beyond it. The boundary from an additional detection from t_0 with $T = 65$ d is depicted green over the whole tracking process. (g) As a function of longitude, area of the largest domain enclosed by advected boundaries within their theoretical Lagrangian coherence horizon.

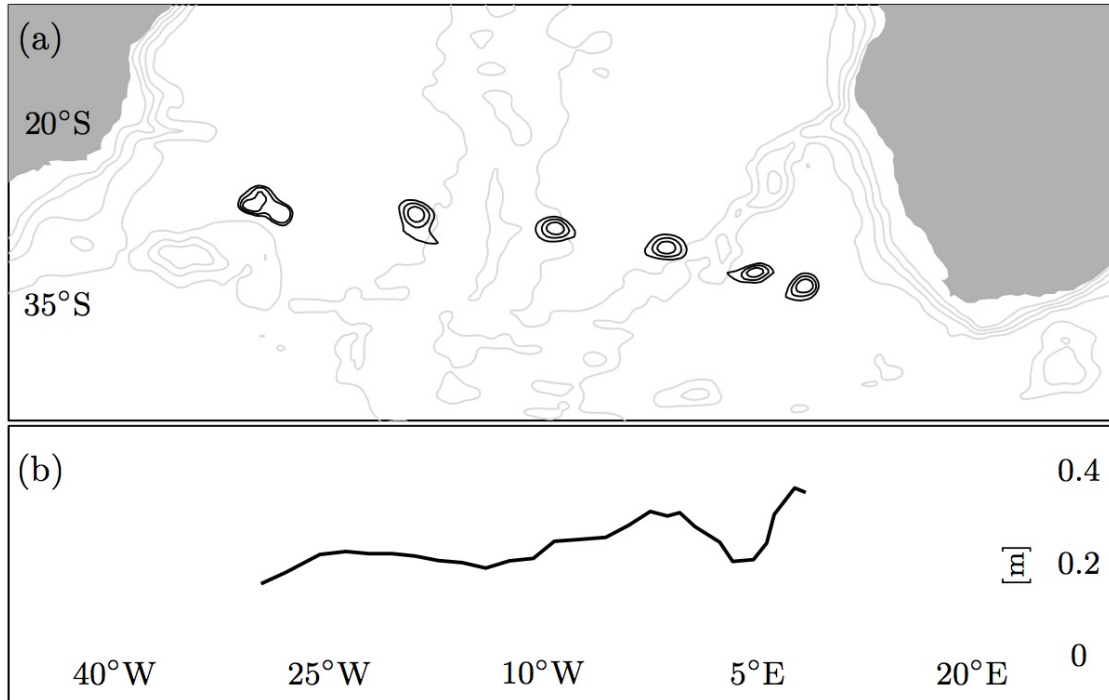


Figure 2. (a) Streamlines of the altimetric sea surface height (SSH) field in each rectangular region indicated in (a–f). (b) As a function of longitude, maximum SSH anomaly associated with the ring.

tional speed of the region, indicating an eddy capable of maintaining a coherent structure [Flierl, 1981]. Second, the anomaly falls from about 35 cm in March 1999 to nearly 20 cm in August 1999, before the ring reaches the Walvis Ridge. Similar behavior for other altimetry-tracked rings within the western Cape Basin was reported by Schouten *et al.* [2000].

However, a change in SSH anomaly does not necessarily imply a corresponding change in material coherence. In fact, the amplitude of the SSH anomaly recovers past the Walvis Ridge, reaching in November 1999 almost 90% of its amplitude in March 1999. Beyond November 1999, the amplitude of the SSH anomaly falls again, at a rate of about 0.9 cm month⁻¹. But meanwhile the ring interior loses material coherence gradually with no interruption.

An increase in the SSH amplitude may nevertheless be indicative of interaction with the bottom topography. *de Steur and van Leeuwen's* [2009] numerical experiments reveal an upward transfer of kinetic energy accompanied by an increase of the SSH amplitude when a baroclinic eddy crosses a meridional ridge. A large vertical extent for the ring can thus be expected, given that the characteristic depth of the Walvis Ridge is over 2 km [Byrne *et al.*, 1995]. Such a large vertical extent is in line too with in-situ hydrographic observations [van Aken *et al.*, 2003].

4. Enduring Lagrangian coherence

While filamentation of the ring is observed starting 30 d after detection on 31 March 1999, a large fraction of the ring's fluid preserves a strikingly compact entity over 2 years of evolution. This is manifested in the evolution of the material loop indicated in green in Fig. 1. This loop is the outermost of a nested family of arclength-reassuring ($\lambda = 1$) loops obtained from a $T = 65$ d calculation. Beyond its theoretical coherence horizon and for nearly 2 years, this 65-d boundary develops only tangential filamentation. More specifically, even after formal coherence is lost, it neither

stretches away from, nor spirals into, the ring core. The 65-d boundary encloses about 55% of the fluid enclosed by the 30-d material boundary on 31 March 1999. Any boundary larger than the 65-d boundary is found to develop long filaments far to the east of the ring as it translates westward beyond 2 months or so. Effectively, however, about 70% of the fluid enclosed by the 30-d boundary is actually seen to evolve quite coherently for about 2 years. This conclusion follows from tracking passive tracers lying in between the 30- and 65-d boundaries.

The enduring Lagrangian coherence of the ring is explained as a consequence of successive short-term Lagrangian coherence regain events. To illustrate this, in Fig. 3a we show (in green) selected advected positions of the 65-d boundary. Overlaid on each we depict (in red) a 30-d boundary identified on the date when the advected 65-d boundary is shown. (An animation including monthly snapshots is supplied as supporting information Movie 2 at <https://www.dropbox.com/s/tl4f5h8n3upuy9j/SI2.mov?dl=0>) For nearly 2 years the advected 65-d boundary is instantaneously closely shadowed by a 30-d boundary, which provides an effective short-term shield to mixing of the fluid near and inside the advected 65-d boundary with the ambient fluid stirred by turbulence. Furthermore, because a shielding boundary is the outermost member of a nested family of coherent material loops that fill up the ring interior, the ring core remains impermeable over such an extended period as well. This is manifested by the incapability of the 65-d boundary to penetrate the ring core by spiralling inward. Such a long-lasting tangential filamentation is found to apply to 65-d through 120-d boundaries. In other words, the material belt delimited by the 65- and 120-d boundaries provides a thick barrier that provides isolation for the fluid inside the 120-d boundary. This accounts for 27% of the total fluid trapped inside the ring, which has a diameter of about 120 km.

Beyond approximately 2 years filamentation of the advected 65-d boundary ceases to be tangential, signaling more intense mixing with the ambient fluid. Consistent with this

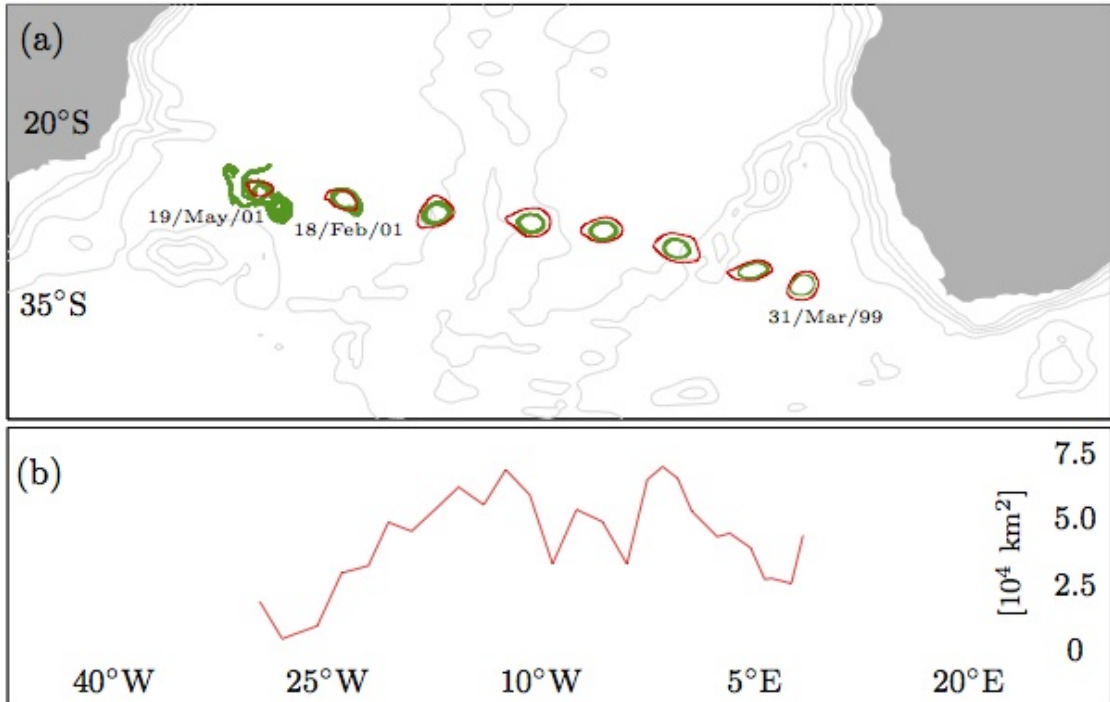


Figure 3. (a) In green, advected images on selected dates of the third-to-outermost material loop in Fig. 1a, corresponding to the Lagrangian ring boundary with coherence time scale $T = 65$ d. In red, shielding boundaries detected from 30- or 15-d integration from the dates shown. (b) Area enclosed by the short-time shielding boundaries as a function of their geographic longitude location.

the 30-d boundaries start to shrink, losing their shielding power, until no 30-d boundary can be detected (Fig. 3b shows the area enclosed by the shielding boundaries as a function of longitude position taken). This happens on 19 May 2001. Beyond this date only a 15-d boundary can be extracted. Eventually by 3 June 2001 no short-term boundary is possible to be identified, the ring detected on 31 March 1999 loses Lagrangian entity completely, and can be declared dead, prior to reaching the South American coast.

Not surprising due to the observer-dependent nature of Eulerian analysis, the demise of the Lagrangian ring cannot be inferred from the inspection of the topology of the SSH field. In fact, a compact region of closed SSH streamlines exists even when the ring has vigorously filamented (cf. left-most SSH contours in Fig. 2a and Fig. 1f). Also, that the area enclosed by the shielding boundaries has shrunk considerably by February 2001 explains why *Froyland et al.* [2015] could not extract any coherent sets beyond February 2001.

Thus the slow decay reported by *Froyland et al.* [2015] is attributed to the occurrence of successive coherence regain events. This enduring Lagrangian coherence is not inferable from a direct application of geodesic eddy detection on a fixed date as done in *Wang et al.* [2015]. Revealing it requires one to apply it on successive dates. The implications of slowly decaying rings for transport are discussed in Section 6 below.

5. Genesis

An attempt was made too to shed light on the genesis process of the ring by applying again geodesic eddy detection on $t_0 = 31$ March 1999, but in backward time.¹ This procedure enabled isolating coherent Lagrangian eddy boundaries only with $T > -60$ d. Because the short-termed forward boundaries were found to provide shielding for the ring over a long time scale, we set $T = -30$ d and performed the analysis around the backward-advected locations of the ring core (taken as the center of mass of the fluid lying inside the

480-d boundary on 31 March 1999). By 30 January 1999, no boundary with $T = -30$ d could be extracted, so we switched to $T = -15$ d and reduced the detection step to two weeks. This led to the isolation of 2 boundaries with $T = -30$ d on 31 and 1 March 1999, and 6 boundaries with $T = -15$ d from 30 January 1999 back to 16 November 1998 every 15 d.

Figure 4 depicts on selected dates these backward boundaries (in red) overlaid on the backward-advected images of the forward boundaries extracted on 31 March 1999 (light blue). The backward boundary on 31 March 1999 is smaller than the outermost forward boundary on that date, which provides only partial shielding for the ring when advected in backward time. Note the filaments stretching away from the ring into the South Atlantic.

A closer look reveals that some filaments spiral inward to the center of the ring. This is evident from the inspection of the backward-advected images of 120-d boundary on 31 March 1999 (depicted in dark blue in Fig. 4 on selected dates). The inward spiraling of this boundary happens at least up to 16 December 1998.

The shielding boundaries shrink considerably past 16 December 1998, and filamentation of the 120-d boundary turns both inward and outward spiraling. By 16 November 1998 the shielding boundary has shrunk considerably and a part of the 120-d boundary is seen to spiral into a swirling structure from which neither forward- nor backward-time coherent material loops are possible to extract. On 1 November 1998 the 120-d boundary takes a highly convoluted filamental structure.

The genesis process thus resembles the demise stage but in reversed time. The ring in question is seen to be the result of a ring-merging event rather than a simple occlusion of, and subsequent pinch off from, the Agulhas retroflection [*Dencausse et al.*, 2010; *Pichevin et al.*, 1999]. Such a merging event occurs right within Cape Cauldron, a highly turbulent region well separated from the Agulhas retroflection

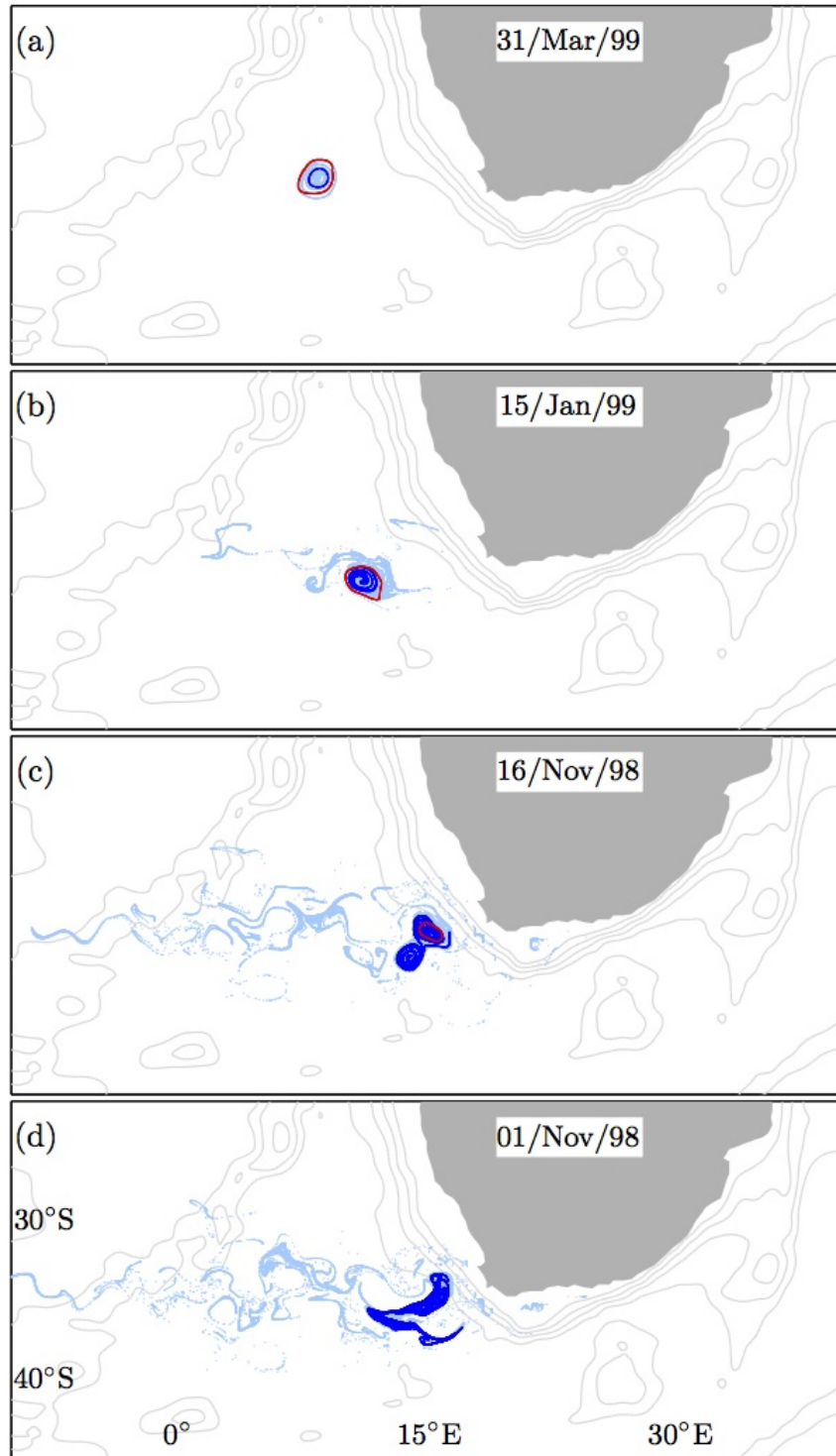


Figure 4. Backward-advected images on selected dates of the ring boundaries in Fig. 1 corresponding to several Lagrangian coherence time scales (all depicted light blue, except the 120-d boundary, shown in dark blue) with the short-term shielding boundary obtained from backward-time integration from the date indicated overlaid (red).

[Boebel *et al.*, 2003]. This is consistent with the observation made by Wang *et al.* [2015] that material Agulhas rings are organized from incoherent fluid away from the Agulhas retroflection. Furthermore, quite a good deal of the fluid (more than 75% as a long backward advection reveals) that ends up forming the ring comes from the South Atlantic.

6. Implications for transport

An important question is how material coherence regain events affect the conclusions of Wang *et al.* [2015] if they were to be verified for all Agulhas rings. A quick computation reveals that rings would carry yearly about 6 Sv ($1 \text{ Sv} = 10^6 \text{ m}^3 \text{ s}^{-1}$) across the South Atlantic. This rough estimate follows from assuming that annually about 3 co-

herent material rings are formed [Wang *et al.*, 2015], and as inferred for the ring investigated here, the diameter of the rings is about 240 km, the coherence response at the surface extends down to 2 km, and 70% of the ring fluid on the detection date is carried well across the subtropical gyre. If we further assume that about 25% of the ring contents are traceable into the Indian Ocean, as is applicable to the ring investigated here, then the Agulhas leakage trapped in rings which is able to traverse the South Atlantic would amount to up to 1.5 Sv.

Overall, the transport results of Wang *et al.* [2015] may be underestimated by one order of magnitude. But the main conclusions of Wang *et al.* [2015] should remain unaltered because Agulhas leakage estimates are still almost an order of magnitude bigger [e.g., Richardson, 2007]. On the other hand, there is large uncertainty around the behavior of the rings below the surface. For instance, according to numerical simulations the vertical structure of a ring may decay much faster than its surface signature [de Steur *et al.*, 2004]. Moreover, Wang *et al.* [2015] showed that only a very small fraction of fluid trapped inside rings detected over the last two decades is eventually picked up by the North Brazil Current. Thus while coherent Lagrangian Agulhas rings provide a direct route for the Agulhas leakage across the subtropical gyre, most of it may be advected incoherently.

The genesis of coherent material rings in the Cape Cauldron also implies a very distinct process of transport of salt by these rings. In particular, while previous observations suggest that Agulhas rings are shed directly from the Agulhas retroflection and experience turbulent mixing thereafter [Boebel *et al.*, 2003; Schouten *et al.*, 2000; Schmid *et al.*, 2003], mixing of the Agulhas leakage with its surrounding occurs before a coherent material ring is actually born. As a result, although a ring may possess sustained material coherence, it will contain a considerable amount of Atlantic water as well [Wang *et al.*, 2015]. However, the amount of salt eventually trapped in rings should not be considered to be small. Indeed, hydrographic records show that the salt anomaly associated with a mature coherent Agulhas ring (180-km diameter and 1.6-km depth) can be as high as 8.4×10^{12} kg [Schmid *et al.*, 2003]. A quick computation, then, reveals that the ring in the present study may transport approximately 10×10^{12} kg of excess salt across the South Atlantic, roughly 15% of the total annual Indian-Atlantic Ocean salt flux [Lutjeharms and Cooper, 1996].

7. Concluding remarks

Application of geodesic eddy detection on a recently investigated Agulhas ring has allowed us to explain its enduring Lagrangian coherence when detected from altimetry using a probabilistic method [Froyland *et al.*, 2015] as a result of the successive occurrence of coherence regain events. These events are characterized by the formation of coherent material loops around the ring, preventing the fluid trapped from mixing with the ambient fluid. These short-term boundaries develop to the west of the Walvis Ridge, likely favored by the more quiescent environmental conditions there than in the Cape Basin [Schouten *et al.*, 2000; Boebel *et al.*, 2003]. The ring is found to lose its material coherence completely as a result of a ring-splitting event after about 2 years of travelling across the subtropical gyre. The genesis of the ring is a result of a ring-merging event rather than a simple occlusion of, and subsequent pinch off from, the Agulhas retroflection. If the enduring Lagrangian coherence of the Agulhas ring scrutinized here were be applicable to all rings detected from the altimetry record, Wang *et al.*'s [2015] annual transport estimates should be increased by one order of magnitude. But even in such a case Wang *et al.*'s

[2015] conclusions about the limited ability of Agulhas rings to carry Agulhas leakage across the South Atlantic would remain valid as these corrected transport estimates would still be much smaller than reported leakage estimates. The contribution of coherent Lagrangian Agulhas rings to the transport of salt is also smaller than estimates by previous studies [van Ballegooyen *et al.*, 1994; Lutjeharms and Cooper, 1996] suggesting that over 95% (more than 70×10^{12} kg year⁻¹) of interbasin salt flux is attributable to rings. Nevertheless, the excess salt associated with a coherent Lagrangian ring may be too large to be neglected, which deserves to be investigated in more detail.

Acknowledgments. The altimeter products were produced by SSALTO/DUCAS and distributed by AVISO with support from CNES (<http://www.aviso.oceanobs>). Our work was supported by NASA through grant NNX14AI85G and NOAA through the Climate Observations and Monitoring Program.

Notes

1. All of the backward-time integration results reported are such that at least 90% reversibility of the initial tracer positions is guaranteed.

References

- Beron-Vera, F. J., Y. Wang, M. J. Olascoaga, G. J. Goni, and G. Haller (2013), Objective detection of oceanic eddies and the Agulhas leakage, *J. Phys. Oceanogr.*, *43*, 1426–1438.
- Beron-Vera, F. J., M. J. Olascoaga, G. Haller, M. Farazmand, J. Triñanes, and Y. Wang (2015), Dissipative inertial transport patterns near coherent Lagrangian eddies in the ocean, *Chaos*, *25*, 087,412, doi:10.1063/1.4928693.
- Boebel, O., J. R. E. Lutjeharms, C. Schmid, W. Zenk, T. Rossby, and C. Barron (2003), The Cape Cauldron: a regime of turbulent inter-ocean exchange, *Deep-Sea Res. II*, *50*, 57–86.
- Byrne, D. A., A. L. Gordon, and W. F. Haxby (1995), Agulhas eddies: A synoptic view using Geosat ERM data, *J. Phys. Oceanogr.*, *25*, 902–917.
- de Steur, L., and P. J. van Leeuwen (2009), The influence of bottom topography on the decay of modeled Agulhas rings, *Deep-Sea Res. I*, *56*, 471–494.
- de Steur, L., P. J. van Leeuwen, and S. S. Drijfhout (2004), Tracer leakage from modeled Agulhas rings, *J. Phys. Oceanogr.*, *34*, 1387–1399.
- Dencausse, G., M. Arhan, and S. Speich (2010), Spatio-temporal characteristics of the Agulhas Current retroflection, *Deep Sea Res. I*, *57*, 1392–1405.
- Flierl, G. (1981), Particle motions in large-amplitude wave fields, *Geophys. Astrophys. Fluid Dyn.*, *18*, 39–74.
- Froyland, G., C. Horenkamp, V. Rossi, and E. van Sebille (2015), Studying an Agulhas ring's long-term pathway and decay with finite-time coherent sets, *Chaos*, *0*, 0–0.
- Haller, G., and F. J. Beron-Vera (2013), Coherent Lagrangian vortices: The black holes of turbulence, *J. Fluid Mech.*, *731*, R4, doi:10.1017/jfm.2013.391.
- Haller, G., and F. J. Beron-Vera (2014), Addendum to 'Coherent Lagrangian vortices: The black holes of turbulence', *J. Fluid Mech.*, *755*, R3.
- Karrasch, D., F. Huhn, and G. Haller (2014), Automated detection of coherent Lagrangian vortices in two-dimensional unsteady flows, *Proc. Royal Soc. A*, *471*, 20140,639.
- Le Traon, P. Y., F. Nadal, and N. Ducet (1998), An improved mapping method of multisatellite altimeter data, *J. Atmos. Oceanic Technol.*, *15*, 522–534.
- Lehahn, Y., F. d'Ovidio, M. Lévy, Y. Amitai, and E. Heifetz (2011), Long range transport of a quasi isolated chlorophyll patch by an Agulhas ring, *Geophys. Res. Lett.*, *38*, L16,610, doi:10.1029/2011GL048588.
- Lutjeharms, J. R. E., and J. Cooper (1996), Interbasin leakage through Agulhas Current filaments, *Deep-Sea Res. I*, *43*(2), 213–238, doi:10.1016/0967-0637(96)00002-7.

- Onu, K., F. Huhn, and G. Haller (2015), LCS Tool: A computational platform for Lagrangian coherent structures, *J. Comp. Sci.*, *7*, 26–36.
- Pichevin, T., D. Nof, and J. R. E. Lutjeharms (1999), Why are there Agulhas rings?, *J. Phys. Oceanogr.*, *29*, 693–707.
- Richardson, P. L. (2007), Agulhas leakage into the Atlantic estimated with subsurface floats and surface drifters, *Deep Sea Res. I*, *54*, 1361–1389.
- Rio, M.-H., and F. Hernandez (2004), A mean dynamic topography computed over the world ocean from altimetry, in situ measurements, and a geoid model, *J. Geophys. Res.*, *109*, C12,032, doi:10.1029/2003JC002226.
- Schmid, C., O. Boebel, W. Zwenk, J. R. E. Lutjeharms, S. L. Garzoli, P. L. Richardson, and C. Barron (2003), Early evolution of an Agulhas ring, *Deep-Sea Res. II*, *50*, 141–166.
- Schouten, M. W., W. P. M. de Ruijter, and P. J. van Leeuwen (2000), Translation, decay, and splitting of Agulhas rings in the southeastern Atlantic Ocean, *J. Geophys. Res.*, *105*, 21,913–21,925.
- van Aken, H. M., A. K. van Veldhoven, C. Veth, W. P. M. de Ruijter, P. J. van Leeuwen, S. S. Drijfhout, C. P. Whittle, and M. Rouault (2003), Observations of a young Agulhas ring, Astrid, during MARE in March 2000, *Deep-Sea Res. II*, *50*, 167–195.
- van Ballegooyen, R.-C., M. L. Gründlingh and J. R. E. Hernandez (1994), Eddy fluxes of heat and salt from the southwest Indian Ocean into the southeast Atlantic Ocean: A case study, *J. Geophys. Res.*, *99*(C7), 14,053–14,070, doi:10.1029/94JC00383.
- Wang, Y., M. J. Olascoaga, and F. J. Beron-Vera (2015), Coherent water transport across the South Atlantic, *Geophys. Res. Lett.*, *42*, 4072–4079, doi:10.1002/2015GL064089.
-
- Y. Wang, RSMAS/OCE, University of Miami, 4600 Rickenbacker Cswy., Miami, FL 33149, USA. (ywang@rsmas.miami.edu)
- F. J. Beron-Vera, RSMAS/ATM, University of Miami, 4600 Rickenbacker Cswy., Miami, FL 33149, USA. (fberon@rsmas.miami.edu)
- M. J. Olascoaga, RSMAS/OCE, University of Miami, 4600 Rickenbacker Cswy., Miami, FL 33149, USA. (jolascoaga@rsmas.miami.edu)